FLOW PAST TWO FINITE-LENGTH WALL-MOUNTED CYLINDERS IN TANDEM ARRANGEMENT AT Re = 200

by

***Xing ZHOU*[a]*, Shifeng WANG*[b]*, and Deming NIE*[a*]**

[a]Institute of Fluid Mechanics, China Jiliang University, Hangzhou, China
[b]Science and Technology Department, Hangzhou Vocational & Technical College, Hangzhou, China

Original scientific paper
https://doi.org/10.2298/TSCI22S1001Z

To investigate the characteristics of flow over two finite-length cylinders in tandem arrangement, numerical simulations were performed using CFD technique for spacing ratios (S = D/d, where d is the diameter of the cylinders and D is the separation gap between the cylinders) between 0.5 and 12 at a Reynolds number of 200. The height-to-diameter ratio (h/d, where h is the height of the cylinders) was fixed at 8. This study primarily focuses on the effects of S and the free ends on the vortical structure behind the cylinders. The S has a significant effect on the Strouhal number and on the lift and drag coefficients of cylinders. The results show extremely different vortex streets at different cylinder heights. With an increase in S, the average drag coefficient of the downstream cylinder increases, whereas that of the upstream cylinder first decreases and then increases. Additionally, as S changes between 4.5 and 5, the average drag coefficient of the two cylinders changes suddenly. The effects of S on Strouhal number and the lift coefficient exhibit a complex behavior.

Key words: *finite-length cylinder, wall-mounted cylinder, tandem arrangement, CFD, vortical structure*

Introduction

The problem of flow around a circular cylinder is widely encountered in engineering practice. Furthermore, the problem of flow around multiple cylinders, as a branch of the problem of flow around a circular cylinder, has become extremely important in the field of fluid mechanics, particularly in wind engineering, hydraulic engineering, and construction engineering. Therefore, it is of great significance to address practical engineering problems, such as wind turbine and bridge construction. It is important to understand the interaction of multiple structures in the flow. In the flow around multiple cylinders, the cylinders interfere with each other. The number, position, and clearance of the cylinders affect each other. The shape and size of the vortex shedding are very different from those of flow around a single cylinder [1]. The basic shape of a structure or component is a circular cross-section, so the tandem double cylinder as a basic example of a multi-structure array that has important research significance and value [2]. It is important to understand the characteristics of the flow around a single cylinder before studying the flow around multiple cylinders, accordingly,

*Corresponding author, e-mail: nieinhz@cjlu.edu.cn

many studies have been conducted on the flow around a single cylinder. Silva *et al*. [3], Ong *et al.* [4], Wang and Shao [5], and Jiang and Cheng [6] investigated the 2-D flow around a single cylinder for different Reynolds number. De and Sarkar [7] investigated the shear flow around an infinite-height circular cylinder in an early 2-D to 3-D transition regime via direct numerical simulations. Maryami *et al*. [8] experimentally investigated the effect of turbulent inflow on the fluctuating pressure on the surface of a cylinder by using a highly instrumented cylinder equipped with several peripheral and spanwise surface pressure transducers. Wang *et al*. [9] investigated the flow mechanism and characteristics of a finite-length cylinder. A large eddy simulation (LES) numerical model and the vortex identification method were used to simulate the flow around a finite-height cylinder, and the results were compared with those of flow around an infinite-length cylinder. It was found that vortex shedding behind a finite-length cylinder was restrained by a downwash vortex at the free end of the cylinder. Jiang and Cheng [10] numerically simulated the effect of a small wire placed in the near wake of the main infinite-length cylinder for different Reynolds number (Re $\leqslant$ 400) and explored the mechanism of the flow field changing from periodic to non-periodic as Reynolds number increased.

As a basic form of flow around multiple cylinders, the flow around two cylinders has been widely investigated in recent years. Currently, research on flow around double cylinders focuses on the effect of cylinder arrangement, distance between cylinders, and Reynolds number on the flow field [11-13]. The flow around 2-D double cylinders in a tandem arrangement has been extensively investigated. Liu *et al*. [14] investigated the flow around 2-D double cylinders in a tandem arrangement at subcritical Reynolds number. Their results show that the wake of the two cylinders exhibits different vortex shedding patterns as the spacing between the two cylinders varies. Sharman *et al*. [15] analyzed the flow around 2-D double cylinders in a tandem arrangement at Re = 100 using an unstructured hybrid CFD code. A critical spacing ratio (*i.e*., the ratio of the distance between the centers of the two cylinders to the diameter of the cylinders) was found between 3.75 and 4 diameters, at which fluctuating forces jumped appreciably. Other studies using 2-D simulations also showed the existence of a critical spacing ratio [16-20]. In addition, Lin *et al*. [21] presented a numerical investigation of the flow-induced vibration around two elastically mounted cylinders in a tandem arrangement at subcritical Reynolds number.

Using the 3-D LES method, Zhou *et al*. [22] investigated the flow around two infinite-length cylinders in tandem at Re = 1000. Their results showed that there was a critical spacing ratio, similar to the 2-D results. Zdravkovich *et al*. [23] experimentally studied the flow past two cylinders in tandem and in a staggered arrangement. They found that the critical spacing ratio D/d (where D is the separation gap between the cylinders and d is the diameter of the cylinders). When D/d was less than the critical spacing ratio, there was no evident vortex shedding in the upstream cylinder. Meneghini *et al*. [24] investigated the incompressible flow around two infinite-length cylinders in tandem and proposed a mechanism to explain the interference phenomenon and its interaction with a 3-D vortex structure in the flow field. Kondo and Matsukuma [25] investigated the flow past two 3-D infinite-length cylinders in a tandem arrangement for Re = 1000. They found that the average drag coefficient of the two cylinders changed suddenly at a spacing ratio of L/d = 3.5~4 (where L is the distance between the centers of the two cylinders). Deng *et al*. [26] investigated the flow around two 3-D infinite-length cylinders in a tandem arrangement for different Reynolds number and spacing ratios. For Re = 220, they found that the critical spacing range is $3.5 < L/d < 4$; beyond this range, the vortex is shed from the upstream cylinder in 2-D. Hu *et al*. [27] investigated the flow around two 3-D infinite-length cylinders in a tandem arrangement at subcritical and supercritical Reynolds number. In addition, Shang *et al*. [28] investigated the flow over two square cylinders in tandem using a 3-D LES model, and Tang *et al*. [29] numerically investigated the transitional behavior of 2-D laminar flows through and around a square array of 100 circular cylinders.

A literature review shows that studies on the flow around two cylinders are mainly focused on 2-D and 3-D infinite-length cylinders. Research pertaining to the flow around 3-D finite-height double cylinders at low Reynolds number values is rare. Therefore, the flow around two finite-length cylinders in a tandem arrangement at Re =200 was investigated in this study, where a change in the flow field was observed by changing the spacing ratio. Two finite-length cylinders with a height-to-diameter ratio of 8 (h/d, where h and d are the height and diameter of the cylinders, respectively) were selected as the study objects. Reynolds number is calculated using d as the reference length. Subsequently, the obtained lift and drag forces, Strouhal number, and wake flow structure of the cylinders were calculated and analyzed.

Problem description and methods

The computational domain as well as some notations used is shown in fig. 1, which presents a diagram of a uniform free stream with speed, U_0, past two finite cylinders in tandem arrangement. The diameter and height of the cylinders are denoted as d and h, respectively (in this study, h/d = 8). The separation gap between the cylinders is D. To ensure a fully developed wake flow in the simulation, the computational domain size was set to be $40d \times 32d \times 24d$ ($L \times W \times H$). The upstream cylinder is located at a distance L_u from the inlet and L_d from the outlet. The upstream and downstream cylinders are referred to as Cylinders 1 and 2, respectively.

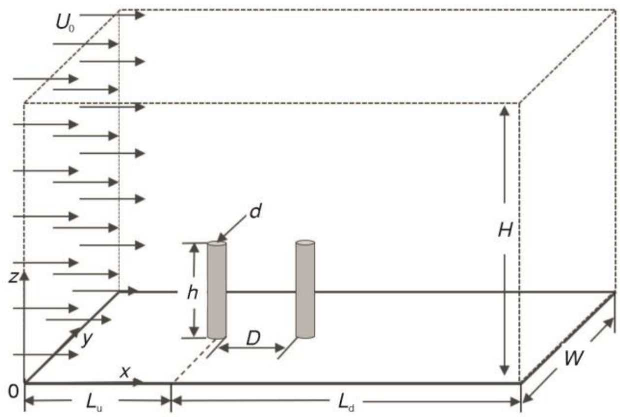

Figure 1. Computational model and some notations used in this study

In the Cartesian co-ordinate system, the continuity and incompressible Navier-Stokes equations for laminar flow are:

$$\frac{\partial u_i}{\partial x_i} = 0 \tag{1}$$

$$\frac{\partial u_i}{\partial t} + u_j \frac{\partial u_j}{\partial x_j} = -\frac{1}{\rho}\frac{\partial p}{\partial x_i} + \nu \frac{\partial^2 u_i}{\partial x_j \partial x_j} \tag{2}$$

where $(x_1, x_2, x_3) = (x, y, z)$ are Cartesian co-ordinates, u_i – the velocity component in the direction x_i, t, ρ, ν, and p represent time, fluid density, kinematic viscosity of air, and pressure, respectively.

In this study, the flow around two finite-length cylinders in a tandem arrangement at Re = 200 is investigated, and the numerical solution is performed using the computational fluid dynamics technique based on finite volume method. A second-order implicit scheme is applied for the temporal discretization. For spatial discretization, a second-order upwind scheme is adopted. The SIMPLEC algorithm is employed to treat the pressure and velocity coupling.

For the model configuration shown in fig. 1, the following boundary conditions are imposed:

– Left surface: Uniform velocity inlet with a flow rate of U_0.
– Right surface: Pressure outlet with a zero relative pressure.
– Bottom and cylindrical surfaces: A wall that satisfies the no-slip boundary condition.
– Other surfaces: The front, back, and top surfaces are set as symmetric surfaces, which satisfy the following equations:

$$\frac{\partial u}{\partial y} = \frac{\partial w}{\partial y} = v = 0 \tag{3}$$

$$\frac{\partial u}{\partial z} = \frac{\partial v}{\partial z} = w = 0 \tag{4}$$

where $(u, v, w) = (u_1, u_2, u_3)$

In addition, an appropriate time step should be selected to satisfy the Courant-Friedrichs-Lewy condition using the following equation [16]:

$$C = \Delta t \sum_{i=1}^{n} \frac{u_i}{\Delta i} \le 1 \tag{5}$$

where C is the Courant number, Δi – the minimum computational grid size in the direction x_i, and Δt – the computational time step. In this study, Δt was set to 0.0005 seconds, which satisfied the requirements.

In the fluid flow numerical simulation, the Reynolds number is a crucial parameter that reveals the state of fluid flow, which is expressed:

$$\mathrm{Re} = \frac{U_0 d}{\nu} \tag{6}$$

When a fluid flows around a cylinder, it exerts a force on the cylinder, which can be divided into two parts: drag in the flow direction and lift perpendicular to the flow direction. To compare the forces acting upon the cylinder, the drag and lift coefficients are introduced to describe the effects of the fluid on the cylinder; they are respectively expressed:

$$C_D = \frac{F_D}{0.5 \rho U_0^2 h d} \tag{7}$$

$$C_L = \frac{F_L}{0.5 \rho U_0^2 h d} \tag{8}$$

where F_D and F_L are the forces parallel and perpendicular to the fluid flow direction on the cylinder, respectively.

Strouhal number is typically used to describe the relationship between the vortex shedding frequency in the flow around a cylinder, the diameter of the cylinder, and the fluid flow velocity. Strouhal number represents the dimensionless vortex-shedding frequency and it is expressed:

$$\mathrm{St} = \frac{fd}{U_0} \tag{9}$$

where f is the dominant vortex shedding frequency, which is generally obtained by performing a fast Fourier transform on the lift coefficient curve.

This study primarily focused on the effects of the spacing ratio and free ends on the structure of the vortex behind the cylinders. To obtain more general results, the spacing ratio $S = D/d$ was defined to describe the spacing between the cylinders.

Validation

In this study, the entire flow field was divided into structural grids, and the entire computational area was divided into seven parts, as shown in fig. 2. When the spacing between the two cylinders is sufficiently large ($S \geqslant 3$), the $3.5d \times 3.5d$ region outside the cylinders is divided into an O-shaped grid for local refinement. When the spacing is small ($S < 3$), the area divided by the O-shaped grid decreased with a decrease in S, fig. 3. The number of meshes in the cross-sectional area increased. To improve the computational efficiency while ensuring computational accuracy, the grid number in other flow fields was decreased gradually with the cylindrical center outward.

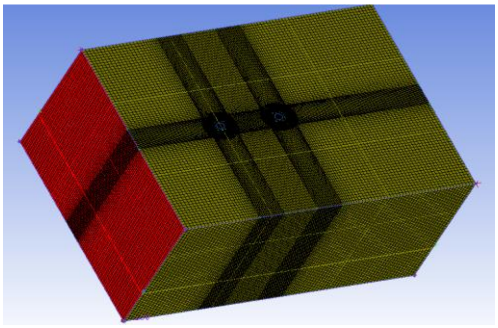

Figure 2. The 3-D grid diagram of flow around two finite-length cylinders in a tandem arrangement

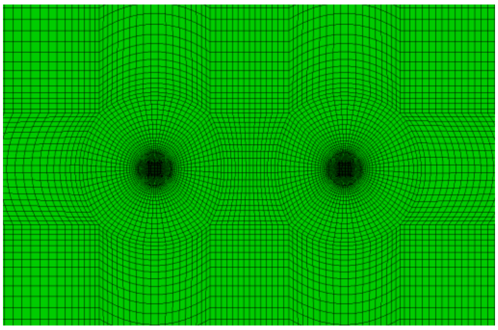

Figure 3. Diagram of O-shaped regions for double cylinders in a tandem arrangement

To examine the influence of the number of grids on the calculation accuracy, when $S = 2$, three sets of meshes with different number of grids were selected for analysis and comparison. The most suitable mesh was selected and the results are listed in tab. 1. As shown, the errors of Strouhal number for Cases 1 in relation to Case 2 and Cases 2 in relation to Case 3 are negligible, therefore, the number of grids can be assumed to have met the irrelevance requirement for the simulation. Considering that the efficiency of the numerical simulation should be improved as much as possible while ensuring that the simulation accuracy meets the requirements, the number of grids was set to 1.76 million, as in Case 2 in tab. 1.

To ensure the accuracy of the computational model, a 2-D physical model at Re = 200 with $S = 3$ for double cylinders in a tandem arrangement was used for comparison. The solution format was set using the SIMPLEC algorithm, a boundary second-order central difference was used, and a laminar model was selected for the calculation. For the same Reynolds number and boundary conditions, Strouhal number was selected and compared with the results of previous studies, and the results are listed in tab. 2. In addition, the flow around a finite-length square cylinder with aspect ratio of 5 (*i.e.*, the ratio of the height of the square cylinder to the width of the square cylinder) at Re = 250 was numerically calculated and compared with previous studies, and the results are listed in tab. 3. The results show that the simulation results of this study are consistent with those of previous studies, and the errors are within an acceptable range, which verifies the accuracy of the computational model used in this study.

Table 1. Irrelevance verification of the number of grids

Case	Number of grids	Strouhal number	Error
1	1.32 million (coarse)	0.0965	–
2	1.76 million (medium)	0.0993	–2.82%
3	2.23 million (fine)	0.1011	–1.78%

Table 2. Comparison of the 2-D Strouhal number results between the current and previous studies

		Strouhal number	Error
Meneghini *et al*. [24]		0.174	0.57%
Fei *et al*. [20]		0.173	1.16%
Present study		0.175	–

Table 3. Comparison of the results for a single finite-length square cylinder between the current and previous studies

	Strouhal number	Error	$\overline{C_D}$	Error
Saha *et al*. [30]	1.30	2.36%	1.26	0.79%
Present study	1.27	–	1.27	–

Numerical results

This study focuses on the flow around two finite-length wall-mounted cylinders at Re = 200 for a spacing ratio S ranging between 0.5 and 12 ($0.5 \leqslant S \leqslant 12$). We provide the drag, lift coefficients and the Strouhal number of the cylinders in this section. The vortical structures at different spacing ratios are also presented. It was found that the lift of the upstream cylinder is close to zero for all S considered, whereas that of the downstream cylinder strongly depends on S reflecting different wake patterns. A total of three basic regimes were summarized according to the spacing gap between cylinders: single bluff-body regime ($0.5 \leq S \leq 2.1$), vortex shedding suppressed regime ($2.2 \leq S \leq 4.9$), and vortex shedding regime ($5 \leq S \leq 12$).

To clearly illustrate the flow of vortex shedding behind the cylinders, the Q-criterion was used to define the vorticity as follows [20]:

$$Q = \frac{1}{2}\left[\left\|S^2\right\| - \left\|\Omega^2\right\|\right] \tag{10}$$

$$S_{ij} = \frac{1}{2}\left(\frac{\partial u_i}{\partial x_j} - \frac{\partial u_j}{\partial x_i}\right) \tag{11}$$

$$\Omega_{ij} = \frac{1}{2}\left(\frac{\partial u_i}{\partial x_j} - \frac{\partial u_j}{\partial x_i}\right) \tag{12}$$

where S_{ij} is the strain tensor and W_{ij} – the vorticity. In 3-D Cartesian co-ordinates, the simplified equation is given by:

$$Q = -\frac{1}{2}\left[\left(\frac{\partial u}{\partial x}\right)^2 + \left(\frac{\partial v}{\partial y}\right)^2 + \left(\frac{\partial w}{\partial z}\right)^2\right] - \frac{\partial u}{\partial y}\frac{\partial v}{\partial x} - \frac{\partial u}{\partial z}\frac{\partial w}{\partial x} - \frac{\partial v}{\partial z}\frac{\partial w}{\partial y} \tag{13}$$

Single bluff-body regime ($0.5 \le S \le 2.1$)

It was found that the wake of the two cylinders exhibits periodic variation at small S ($0.5 \leqslant S \le 2.1$). Figure 4 shows the time series of the lift coefficients of both cylinders at S = 1.5. The case of a single cylinder at the same Reynolds number is also included. It is clearly seen that the downstream cylinder experiences a much higher lift as compared to the upstream one. In fact, the lift coefficient is nearly zero for the upstream cylinder, suggesting that no significant vortex shedding occurs. Furthermore, the amplitude of the lift coefficient of the downstream cylinder is nearly twice that of a single cylinder, as indicated in fig. 4.

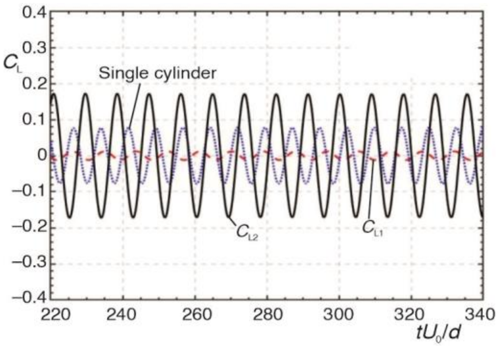

Figure 4. Time history of the lift coefficients for two cylinders at S = 1.5; the case of a single cylinder is also included for comparison

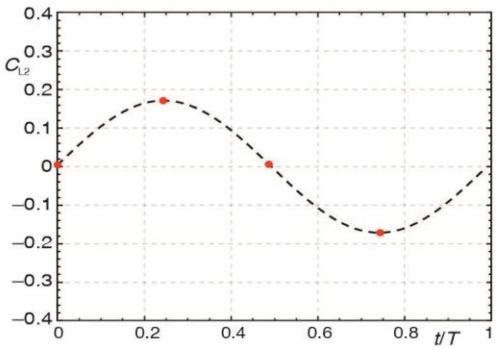

Figure 5. Time history of the lift coefficient for cylinder 2 (C_{L2}) during one period at S = 1.5

We choose four representative times, *i.e.*, t = 0, 0.25T, 0.5T, and 0.75T (where T = 1/St denotes the dimensionless vortex shedding period), as indicated in fig. 5, and show the corresponding vortical structures in fig. 6. Note that the vorticity contours in a spanwise plane (z = 0.5h) and a streamwise plane (y = 0.5W) are presented in the left and right columns in fig. 6, respectively. They illustrate the top-view and front-view of the 3-D flow structures, respectively. The results of a single cylinder are also presented in fig. 7. Three vortex streets are generated behind the cylinders on the plane of z = 0.5h, fig. 6-left, which differs from the 2-D case. Note that the two outmost vortex streets show stronger vorticity as compared with the middle one. More significantly, the vorticity contours in the streamwise plane (y = 0.5W) provide a close view on the evolution of the vortex structures resulting from the wall-mounted cylinders, fig. 6-right. A primary vortex shed from the downstream cylinder, fig. 6(a)-right, is seen to drift away from it, fig. 6(b)-right, and then split into two small vortices, fig. 6(c)-right, resulting in two vortex streets in the wake. Note that the primary vortex is small once it is formed, figs. 6(b)-right and 6(d)-right, and grows quickly, giving rise to a positive or negative lift of the downstream cylinder as indicated in fig. 5. In particular, another vortex street resulting from the bottom wall is also visible, fig. 6-right, resulting in a typical wake pattern consisting of three vortex streets. This is unique for the case of wall-mounted cylinders. In comparison with the downstream cylinder, no visible vortex shedding is seen from the upstream one because of small separation between them, as shown in fig. 6-right. This observation is in accord with fig. 4. On the other hand, the vortical structures shown in fig. 6 are similar to those of a single cylinder, fig. 7, suggesting that the two cylinders at a close separation act like a single bluff-body in the flow. However, the size of the primary vortex shed from the two cylinders is considerably larger than that from a single one. This leads to the fact that the downstream cylinder experiences a significant larger lift than a single cylinder, fig. 4. Another significant difference may be the occurrence of vortex split seen for a single cylinder in the spanwise plane, fig. 7-left, leading to three vortex streets with the middle one showing stronger vorticity.

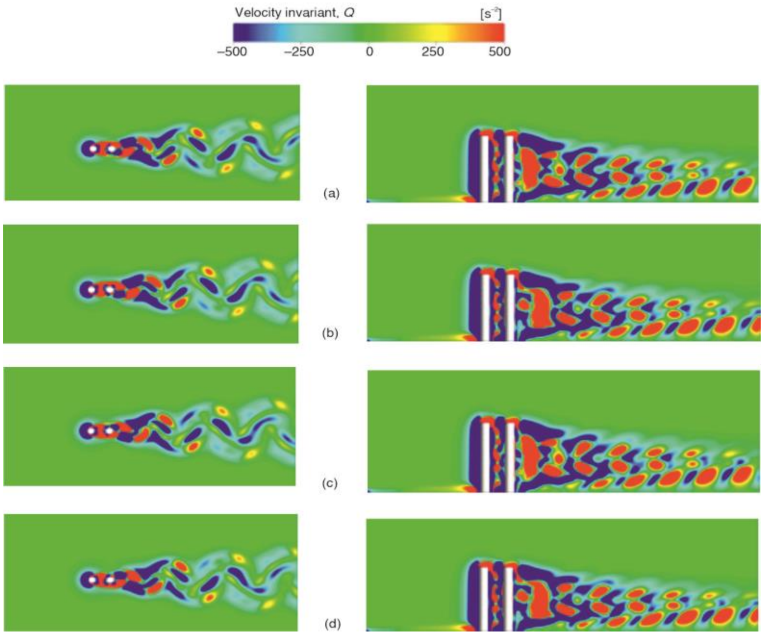

Figure 6. Instantaneous contours of the vorticity on a spanwise plane (z/h = 0.5) (left) and a streamwise plane (y/W = 0.5) (right) at S = 1.5 during one period; (a) t = 0, (b) t =0.25T, (c) t = 0.5T, and (d) t = 0.75T; Note that T denotes the period of vortex shedding

To illustrate the influence of the free end on the wake, the instantaneous vorticity contours at different heights are shown in fig. 8 for S = 1.5 at t = 0 (corresponding to C_{L2} = 0 in fig. 5). It is visible that three vortex streets are formed behind the cylinders at z = 0.25h and 0.5h, as shown in figs. 8(a) and 8(b). As z increases, the number of vortex streets decreases due to the presence of the free end. For instance, two vortex streets are seen at z = 0.75h, fig. 8(c), whereas no vortex street is seen at z = 0.875h, fig. 8(d). The primary reason is that the *downwash* vortex at the free end suppresses the flow separation at large heights. This unique phenomenon is primarily responsible for smaller drag coefficients of wall-mounted finite-length cylinders as compared to that of an infinite-length or 2-D cylinder, as indicated in fig. 23.

Vortex shedding suppressed regime (2.2 ⩽ S ≤ 4.9)

For S ⩾ 2.2, our computations indicate that the wake of the cylinders becomes nonperiodic and the vortex shedding is suppressed. Figure 9 shows the lift coefficients of both

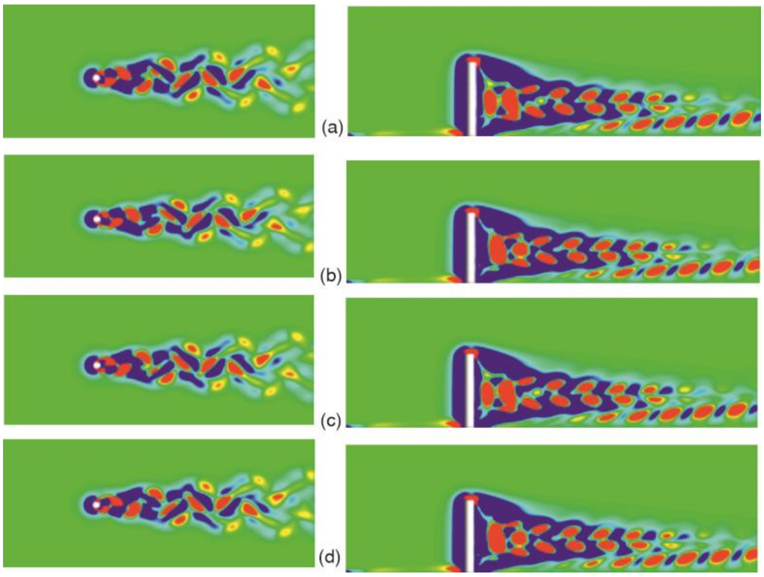

Figure 7. The same as fig. 6 except for a single cylinder; (a) t = 0, (b) t =0.25T, (c) t = 0.5T, and (d) t = 0.75T

cylinders at S = 2.5. As compared with fig. 4, it is seen that the downstream cylinder experiences a significant smaller lift as S increases from 1.5 to 2.5, whereas the upstream cylinder remains the same. The corresponding vortical structures are provided in fig. 10. The presence of the upstream cylinder has a negative effect on the vortex shedding of the downstream cylinder, as can be seen from the vorticity contours on the spanwise plane, fig. 10-left. That is, the vortex generated on the upstream cylinder extends backward and finally attaches on the surface of the downstream cylinder, suppressing the vortex growth and shedding. This could be illustrated by comparing both the number of vortex streets and the wake area on the spanwise plane between S = 1.5, fig. 6-left and 2.5, fig. 10-left. Furthermore, the vorticity contours on the transverse plane, fig. 10-right, show no primary vortex instead of two small vortices shed from the downstream cylinder, unlike the case of S = 1.5, fig. 6-right. This is primarily responsible for a much smaller C_{L2} at S = 2.5 as compared with that at S = 1.5, fig. 4. However, for the upstream cylinder, no visible vortex shedding is seen due to the presence of the downstream cylinder, fig. 10-right, either.

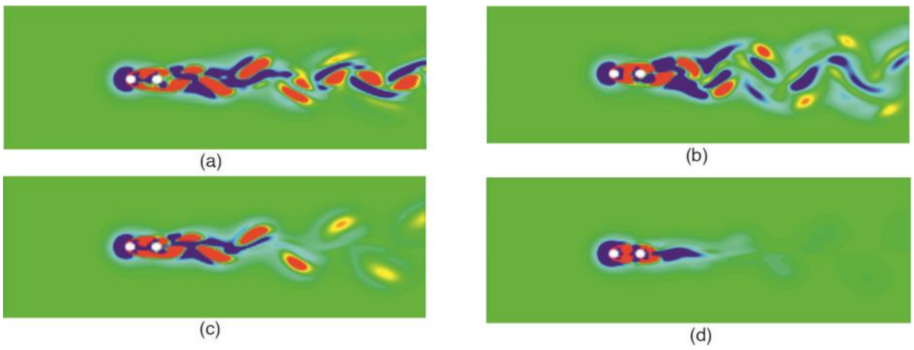

Figure 8. Instantaneous contours of the streamwise vorticity for two cylinders at S = 1.5 at different heights; (a) z = 0.25h, (b) z = 0.5h, (c) z = 0.75h, and (d) z = 0.875h

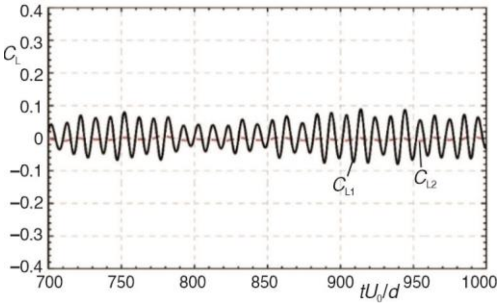

Figure 9. Time history of the lift coefficients for the two cylinders at *S* = 2.5

The vortex shedding from the downstream cylinder is suppressed more significantly as the spacing gap increases, especially when S is between 4.5 and 4.9. As shown in fig. 11, the lift coefficient of the downstream cylinder approaches zero at S = 4.5. To illustrate this behavior more clearly, we present the instantaneous vorticity contours on the spanwise plane (left) and the streamwise plane (right) at a time when C_{L2} is zero in fig. 12, respectively. Note that no substantial difference is seen in the vortex structures at other times. Two symmetrical vortices are generated on the upstream cylinder which extends to the downstream one, fig. 12-left. As a result, the vortex shedding from the downstream cylinder is largely suppressed in terms of both the vorticity strength and the wake area, fig. 12-left. More significantly, the vorticity contour on the streamwise plane shows no visible vortex shed from the downstream cylinder, fig. 12-right, differing from the case of S = 1.5, fig. 6-right, or S = 2.5, fig. 10-right. This causes a lift close to zero for the downstream cylinder.

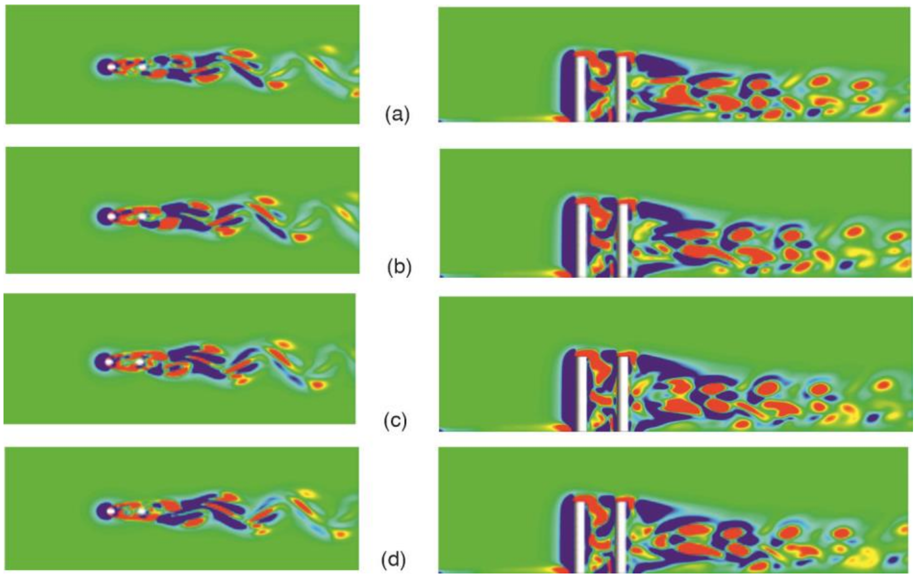

Figure 10. The same as fig. 6 except for *S* = 2.5; (a) *t* = 0, (b) *t* =0.25*T*, (c) *t* = 0.5*T*, and (d) *t* = 0.75*T*

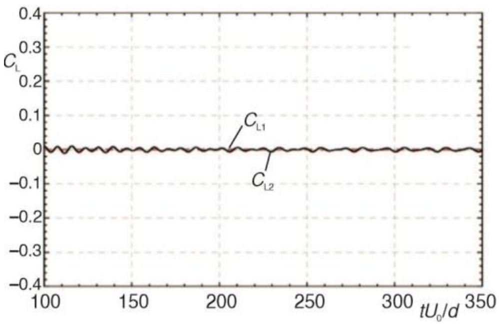

Figure 11. Time history of the lift coefficients for the two cylinders at *S* = 4.5

Vortex shedding regime (5 ≤ S ≤ 12)

The vortex shedding of the downstream cylinder may take place as the spacing gap fur-

Figure 12. Instantaneous contours of the streamwise vorticity on a spanwise plane (z/h = 0.5); (a) and a transverse plane (y/W = 0.5) and (b) at S = 4.5

ther increases. Figure 13 shows the lift coefficients of the two cylinders at S = 5, illustrating a periodic wake pattern with strong oscillations. In comparison with fig. 11, a sudden change in the vortical structures is assumed to occur as S increases from 4.5 to 5. Similar to fig. 6, we show the instantaneous vorticity contours at S = 5 in fig. 14. On the spanwise plane (z = 0.5h), the vortex is seen to shed from the upstream cylinder, fig. 14-left, because the separation gap is large enough for its development and shedding. This noticeably change the situation of the downstream cylinder. That is, three vortex streets are visible showing strong vorticity strength, fig. 14-left. The vorticity contours on the streamwise plane (y = 0.5W) also indicate the occurrence of significant vortex shedding from the downstream cylinder.

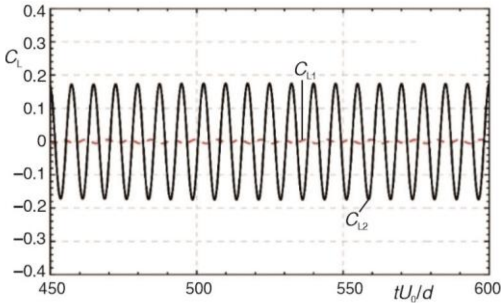

Figure 13. Time history of the lift coefficients of the two cylinders at S = 5

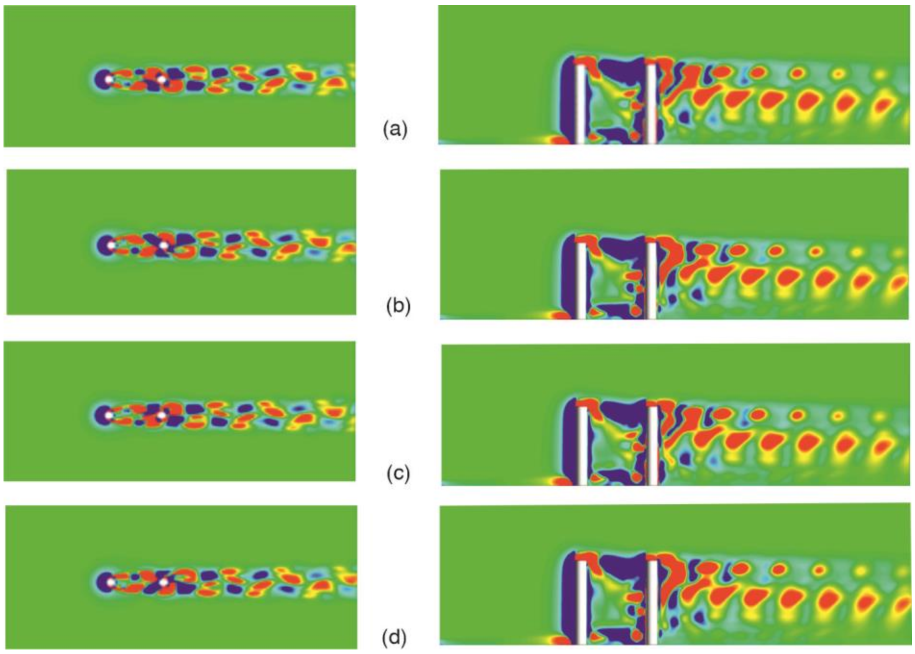

Figure 14. The same as fig. 6 for S = 5;
(a) t = 0, (b) t =0.25T, (c) t = 0.5T, and (d) t = 0.75T

Similar to the case of S = 1.5, fig. 6, a primary vortex is seen to form and grow on the downstream cylinder, fig. 14(a)-right and 14(b)-right, which splits into two small vortices once it is shed, fig. 14(c)-right and 14(d)-right, resulting in two vortex streets in the wake. However, distinct differences can be found in the vortical structures between the cases of S = 1.5 and S = 5. First, in the spanwise plane, the wake area is much larger at S = 1.5, fig. 6-left, than that at S = 5, fig. 14-left. More importantly, a vortex is clearly seen to split into two vortices once it is shed at S = 5. Second, it can be observed from the streamwise plane (y = 0.5W) that the vortex sheds from the middle part of the downstream cylinder at S = 1.5, fig. 6-left, which, however, sheds from its upper part at S = 5, fig. 14-left. This suggests that the lift force is primarily experienced by the middle part of the downstream cylinder at small S and by its upper part at large S. In particular, the *downwash* effect of the free end is not dominant as that seen at S = 1.5. Finally, there are noticeable vortices generated from the wall at S = 1.5, however, they are almost invisible at S = 5. Therefore, only two vortex streets are visible in the streamwise plane for S = 5. This is also true for S > 5.

To provide more insights into our 3-D analysis, we simulated the same problem for 2-D settings. Figure 15 shows the time history of the lift coefficients of two 2-D cylinders for S = 5 at Re = 200. It is clearly seen that the upstream cylinder experiences a considerably larger lift, fig. 15, as compared to its 3-D counterpart, fig. 13. The vorticity contours in the spanwise plane, fig. 14-left, shows visible vortex shedding from the upstream cylinder, which is similar to fig. 16 showing the instantaneous wake around the 2-D cylinders. However, no primary vortex shedding is seen in the streamwise plane, fig. 14-right. Therefore, the upstream cylinder experiences negligible lift force in our 3-D analysis. This is unique for the case of finite-length wall-mounted cylinders, demonstrating the necessity of 3-D simulations. In addition, as compared with the 3-D simulation results, fig. 14-left, the 2-D vorticity contour exhibits a more regular wake pattern, with two vortex streets formed in the flow field, fig. 16.

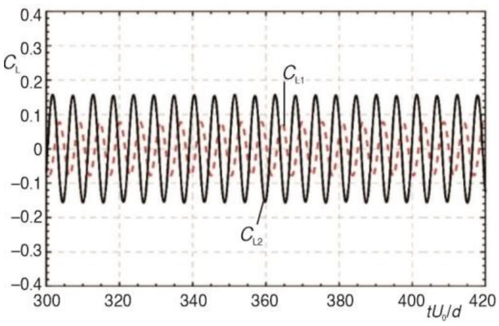

Figure 15. Time history of the lift coefficients for two 2-D cylinders at S = 5

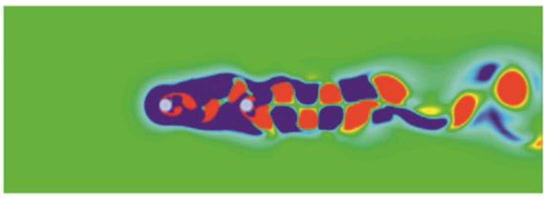

Figure 16. Instantaneous contour of the vorticity around two 2-D cylinders at S = 5

Our simulations indicate that the vortex shedding is enhanced as the wake loses its periodicity when $S \geq 5.3$. Figures 17 and 18 present the numerical results for S = 5.5. The amplitude of C_{L2} is seen to exceed 0.2, fig. 16, obviously larger than both cases of S = 1.5, fig. 4, and S = 5, fig. 13. The time history of C_{L2} also indicates the vortex shedding is nonperiodic at S = 5.5. As shown in fig. 18-left, a vortex shed from the upstream cylinder drifts downstream and merges with another vortex generated on the downstream cylinder, leading to a larger vortex. This process is similar to the case of S = 5, fig. 14-left. However, no vortex split is seen at S = 5.5, resulting in two vortex streets behind the cylinders, similar to the 2-D case, fig. 16.

The vorticity contours in the streamwise plane show enhanced vortex shedding in terms of the vorticity strength and the size of vortex as compared with the case of S = 5, fig. 14-right, as shown in fig. 18-right. A vortex shed from the upstream cylinder is seen to attach on the downstream cylinder, figs. 18(a)-right and 18(c)-right, which finally merges with another vortex generated on the downstream cylinder, figs. 18(b)-right and 18(d)-right. This results in a very long vortex with a length similar to the height of the cylinders. As the vortex is shed from the downstream cylinder, a considerably large lift with positive sign, fig. 18(b) or negative sign, fig. 18(d) is imposed on the cylinder. The streamwise vorticity is also characterized by two significant vortex streets behind the downstream cylinder.

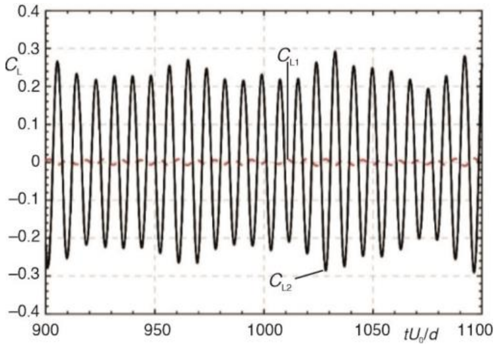

Figure 17. Time history of the lift coefficients for two cylinders at S = 5.5

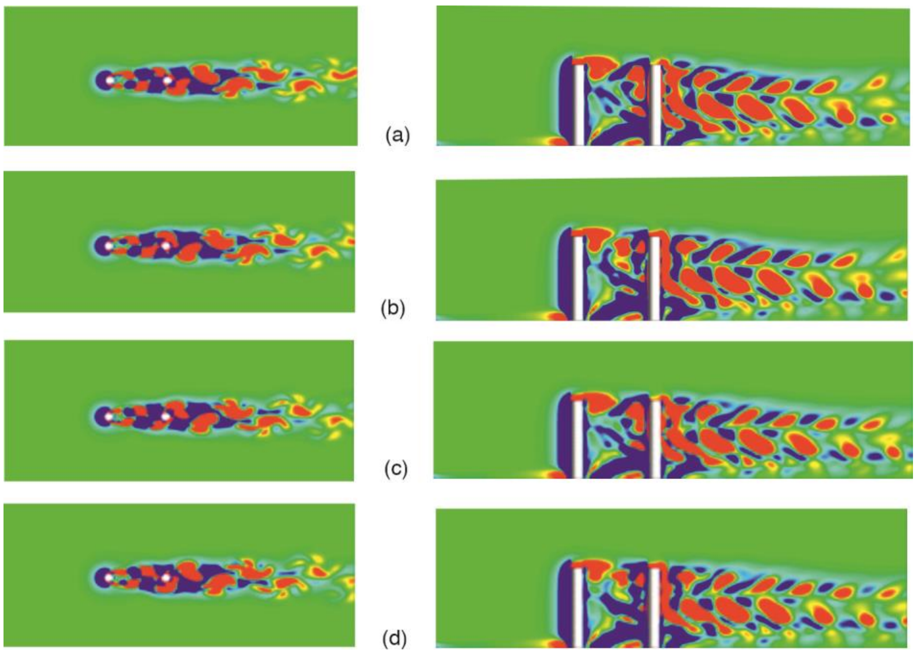

Figure 18. The same as fig. 6 for S = 5.5; (a) t = 0, (b) t =0.25T, (c) t = 0.5T, and (d) t = 0.75T

The wake regains periodicity when the separation gap of the cylinders is large enough, *e.g.*, $S \geq 10$. Figure 19 shows the lift coefficients of the cylinders at S = 12, the largest spacing gap considered. It is seen from fig. 19 that both C_{L1} and C_{L2} are similar to those at S = 5, fig. 13. In particular, the upstream cylinder still experiences a negligible lift at this large separation gap. By contrast, distinct differences in the vortical structures between the two cases are observed as shown in fig. 20. Due to the large separation, a vortex shed from the upstream cylinder is seen to split into two vortices before it attaches on the downstream one, fig. 20-left, differing from the case of S =5, fig. 14-left. Accordingly, one of the two vortices

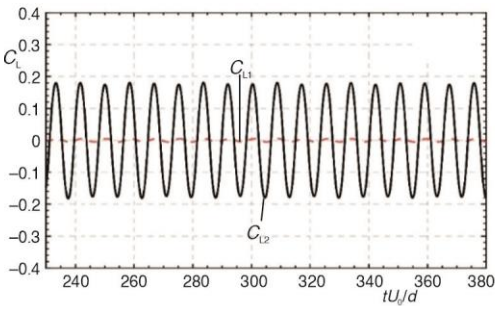

Figure 19. Time history of the lift coefficients of the two cylinders at *S* = 12

is seen to spread and drift aways from the cylinders, resulting in two outmost vortex streets, whereas the other one comes close to the downstream cylinder and attaches on it, fig. 20-left. In total, three vortex streets are seen in the spanwise plane, fig. 20-left, which, however, are different from those at $S = 5$, fig. 14-left, in terms of the vortex shape and the wake area.

As shown in fig. 20-right, the wake pattern behind the downstream cylinder is similar to that of a single cylinder as shown in fig. 7-right, suggesting that the influence of the upstream cylinder is significantly decreasing because of large separation gap. However, the vortex shed from the downstream cylinder is much longer than that from a single one. The reason is mentioned as above: part of the vortex shed from the upstream cylinder merges with the vortex generated on the downstream one. This gives rise to a larger lift for the downstream cylinder, fig. 19, as compared to that of a single cylinder, fig. 4.

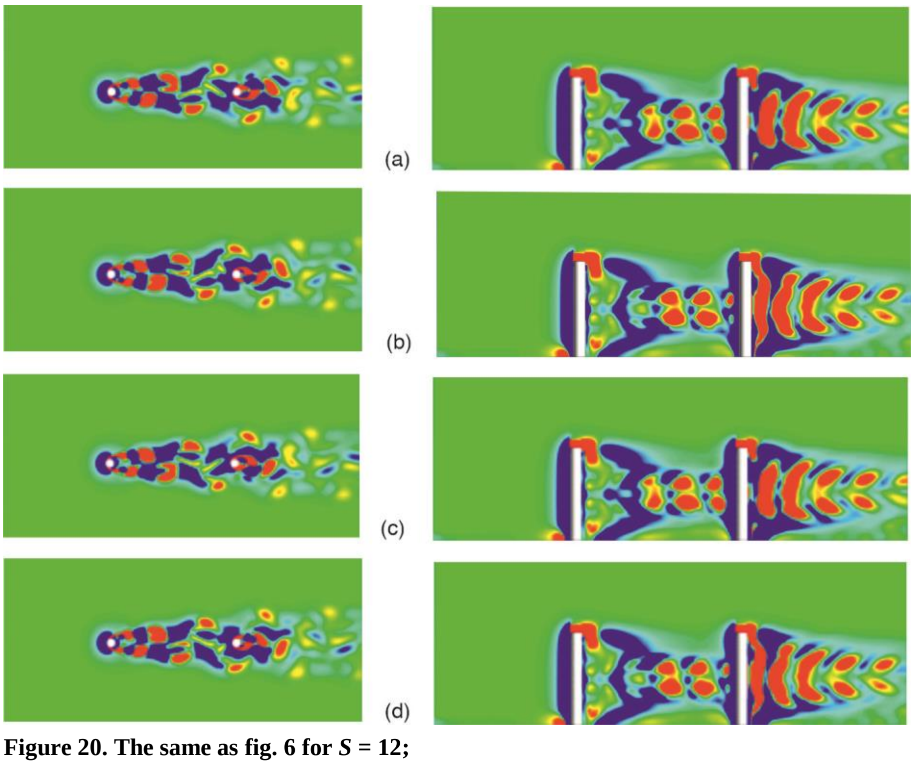

Figure 20. The same as fig. 6 for *S* = 12; (a) *t* = 0, (b) *t* =0.25*T*, (c) *t* = 0.5*T*, and (d) *t* = 0.75*T*

Strouhal number and drag coefficient

Figure 21 summarizes the dependence of the Strouhal number on the separation gap between cylinders. The result of a single cylinder is also shown in the figure. We indicate the periodicity of the wake in fig. 21. It is seen that the Strouhal number decreases rapidly from 0.132 to 0.1 as S increases from 0.5 to 2.1 (corresponding to the single bluff-body regime). Note that the value of Strouhal number is close to 0.13 for the case of a single cylinder. In the vortex shedding suppressed regime ($2.2 \leq S \leq 4.9$), the Strouhal number increases quickly and then reduces to 0.13. After that ($S \geq 5$), the effect of the separation gap on the Strouhal number is nearly negligible irrespective of the periodicity. To provide a direct comparison, the previous 2-D results [17, 31] are shown in fig. 22, which illustrates similar variation of Strouhal number with S except that the magnitude of Strouhal number is much larger for the 2-D case. This difference is primarily caused by the presence of the wall as well as the free end for the present 3-D case. Note that a 2-D cylinder can be considered as an infinite-length 3-D cylinder.

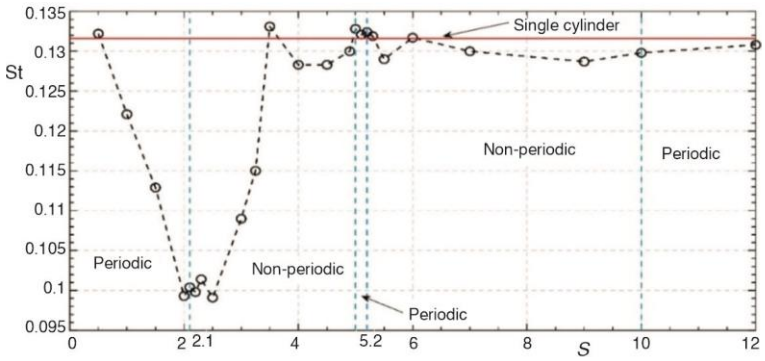

Figure 21. The Strouhal number as a function of *S* for the present 3-D analysis

We also summarize the averaged drag coefficients of both cylinders as a function of the separation gap in fig. 23. The drag coefficient of the upstream cylinder is seen to decrease as S varies from 0.5 to 4.9 and then increases slowly as S varies from 5 to 12. For the downstream cylinder, the effect of S is more significant, as shown in fig. 23. The value of C_{D2} increases from –0.12 to 0.2 as S increases from 0.5 to 4.9. Particularly, a sudden increase in C_{D2} is seen when S = 5, at which the vortex shedding from the downstream cylinder occurs. Similarly, the C_{D2} exhibits another sudden increase at S = 5.5 when the vortex shedding is enhanced (see also fig. 18). In addition, both drag coefficients are smaller than that of a single cylinder for the whole separation gap range considered ($0.5 \leq S \leq 12$).

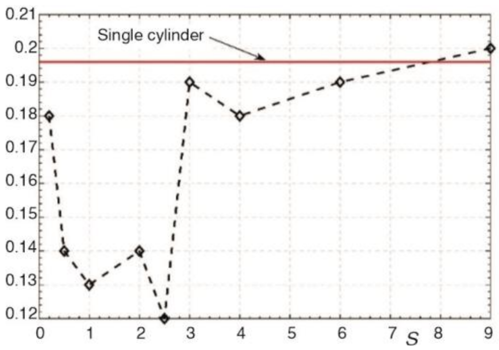

Figure 22. The same as fig. 21 for previous 2-D analysis [17]; the result of a single cylinder is obtained from Qu *et al.* [31]

In comparison with the 3-D case, the influence of S is more significant on both C_{D1} and C_{D2} for the 2-D case, as shown in fig. 24. As S varies from 0.2 to 9, the value of C_{D1} approximately increases from 0.9 to 1.3. In particular, a noticeably sudden increase in C_{D2} is seen at S = 3 when the vortex shedding from the upstream cylinder occurs [17]. At S = 9, the upstream cylinder experiences a drag similar to that of a single cylinder, as shown in fig. 24.

For both 2-D and 3-D cases, C_{D1} is always larger than C_{D2} because the downstream cylinder is shielded from the oncoming flow by the upstream one.

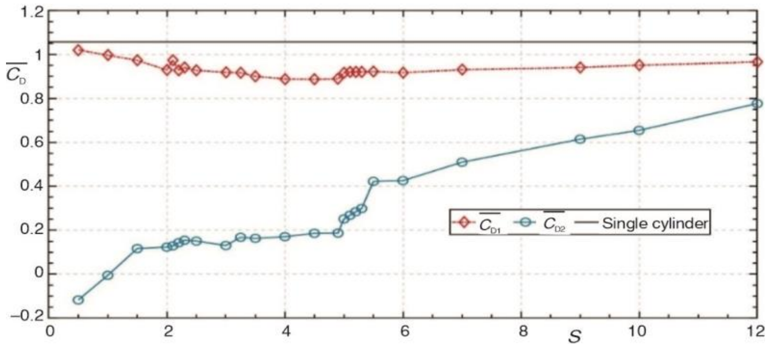

Figure 23. The averaged drag coefficient as a function of *S* for the present 3-D analysis

Conclusion

The numerical simulations and study of the flow around two finite-height cylinders in a tandem arrangement at Re = 200 were performed using the CFD technique. We focused on the changes in the force and flow field of the cylinders for a spacing ratio between 0.5 and 12. Based on the results, the following conclusions are drawn.

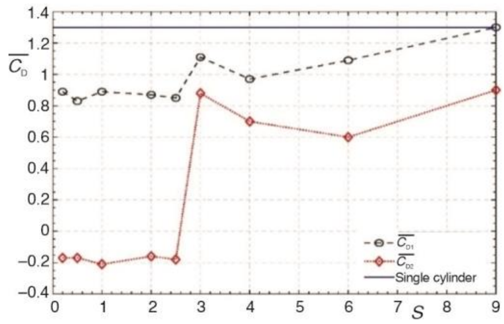

Figure 24. The same as fig. 23 for previous 2-D analysis [15]; the result of a single cylinder is obtained from Qu *et al*. [29]

- Unlike the infinite-height cylinder case, the number of vortex streets was reduced at locations close to the free end of the finite-length cylinders. The reason for this phenomenon is that the *downwash* vortex at the free end of the cylinders suppresses the flow.
- When *S* is less than 2.1 or greater than 10, the entire flow field exhibits a periodic variation. For the former, there is almost no vortex shedding in the upstream cylinder, and the two cylinders can be considered as a single one. For the latter, the periodic behavior is because the distance between the two cylinders is sufficiently large, and the interaction between them is reduced, so the flow field exhibits periodicity again.
- When *S* is between 0.5 and 12, the Strouhal number of the upstream cylinder is the same as that of the downstream cylinder. There are four *St* change phases. In Phase 1, when *S* is very small (*S* = 0.5), Strouhal number is similar to that of a single cylinder, and as *S* increases, Strouhal number decreases until *S* reaches 2. In Phase 2, when *S* is between 2 and 2.5, Strouhal number is almost the same. In Phase 3, when *S* is greater than 2.5, Strouhal number suddenly increases and continues to increase until *S* reaches 3.5. Finally, in Phase 4, when *S* is greater than 3.5, Strouhal number is close to the Strouhal number of a single cylinder.
- When *S* is between 0.5 and 12, the average drag coefficient, $\overline{C_D}$, of the upstream cylinder is always larger than that of the downstream cylinder. The $\overline{C_{D1}}$ first decreases and then increases as *S* increases, and the inflection point is *S* = 4.9. The $\overline{C_{D2}}$ increases as *S* increases,

when S is very small (S = 0.5), $\overline{C_{D2}}$ is negative. When S is between 0.5 and 1.5, and when S is approximately 4.9, $\overline{C_D}$ changes suddenly. The reason for the drastic change in $\overline{C_D}$ is the flow separation enhancement.

Acknowledgment

This work was supported by the National Natural Science Foundation of China (Nos. 11972336 and 12132015).

Reference

[1] Lin, L., *et al*., Numerical simulation of the characteristics and interaction of flow around side-by-side arranged circular cylinders, *Chinese journal of applied mechanics*, *38* (2021), 2, pp. 844-850
[2] Alam, M. M., *et al*., Fluctuating fluid forces acting on two circular cylinders in a tandem arrangement at a subcritical Reynolds number, *Journal of Wind Engineering and Industrial Aerodynamics*, *91*(2003), 1-2, pp.139-154
[3] Silva, A., *et al*., Numerical simulation of two-dimensional flows over a circular cylinder using the immersed boundary method, *Journal of Computational Physics*, *189* (2003), 2, pp. 351-370
[4] Ong, M. C., *et al*., Numerical simulation of flow around a smooth circular cylinder at very high Reynolds numbers, *Marine Structures*, *22* (2009), 2, pp.142-153
[5] Wang, Y. L., Shao, X. M., Study on flow of power-law fluid through an infinite array of circular cylinders with immersed boundary-lattice Boltzmann method, *Thermal Science*, *16* (2012), 5, pp.1451-1455
[6] Jiang, H., Cheng, L., Large-eddy simulation of flow past a circular cylinder for Reynolds numbers 400 to 3900, *Physics of Fluids*, *33* (2021), 3, 034119
[7] De, A. K., Sarkar, S., Wake events during early three-dimensional transition of a circular cylinder placed in shear flow, *Physics of Fluids*, *32* (2020), 5, 053603
[8] Maryami, R., *et al*., Turbulent flow interaction with a circular cylinder, *Physics of Fluids*, *32* (2020), 1, 15105
[9] Wang, X., *et al*., Numerical Simulation of three-dimensional flow around a circular cylinder of finite length, *Chinese Journal of Ship Research*, *13* (2018), 2, pp.27-34
[10] Jiang, H., Cheng, L., Transition to chaos in the cylinder wake through the Mode C flow, *Physics of Fluids*, *32* (2020), 1, 14103
[11] Sumner, D., Two circular cylinders in cross-flow: A review, *Journal of Fluids and Structures*, *26* (2010), 6, pp. 849-899
[12] Zdravkovich, M. M., The effects of interference between circular cylinders in cross flow, Journal of Fluids and Structures, 1 (1987), 2, pp. 239-261
[13] Xu, G., Zhou, Y., Strouhal numbers in the wake of two inline cylinders, Experiments in Fluids, 37 (2004), 2, pp. 248-256
[14] Liu, J. W., *et al*., Numerical simulation of flow around two tandem circular cylinders of equal diameter, *Periodical of Ocean University of China*, *43* (2013), 12, pp. 92-97
[15] Sharman, B., *et al*., Numerical predictions of low Reynolds number flows over two tandem circular cylinders, *International Journal for Numerical Methods in Fluids*, *47* (2005), 5, pp. 423-447
[16] Wei, Z., *et al*., Unsteady characteristics of low-Re flow past two tandem cylinders, *Theoretical & Computational Fluid Dynamics*, *32* (2018), 4, pp. 475-493
[17] Slaouti, A., Stansby, P. K., Flow around two circular cylinders by the random-vortex method, *Journal of Fluids and Structures*, *6* (1992), 6, pp. 641-670
[18] Carmo, B. S., Meneghini, J. R., Numerical investigation of the flow around two circular cylinders in tandem, *Journal of Fluids and Structures*, *22* (2006), 6-7, pp. 979-988
[19] Ghadiri, *et al*., Numerical simulation of flow over circular cylinders in tandem arrangement, *Journal of Hydrodynamics*, *23* (2011), 1, pp. 114-126
[20] Fei, B. L., *et al*., Numerical simulation of flow over two tandem cylinders, *Journal of Southwest University for Nationalities* (Natural Science Edition), *33* (2007), 2, pp. 376-380
[21] Lin, K., *et al*., Numerical investigation of flow-induced vibrations of two cylinders in tandem arrangement with full wake interference, *Physics of Fluids*, *32* (2020), 1, 15112
[22] Zhou, Q., *et al*., Numerical study of wake and aerodynamic forces on two tandem circular cylinders at $Re = 10^3$, *Physics of Fluids*, *31* (2019), 4, 045103

[23] Zdravkovich, M. M., Review of flow interference between two circular cylinders in various arrangements, *Journal of Fluids Engineering*, *99* (1977), Dec., pp. 618-633
[24] Meneghini, J. R., *et al*., Numerical simulation of flow interference between two circular cylinders in tandem and side-by-side arrangements, *Journal of Fluids and Structures*, *15* (2001), 2, pp. 327-350
[25] Kondo, N., Matsukuma, D., Numerical simulation for flow around two circular cylinders in tandem, *International Journal of Computational Fluid Dynamics*, *19* (2005), 4, pp. 277-288
[26] Deng, J., *et al*., Three-dimensional flow around two circular cylinders in tandem arrangement, *Fluid Dynamics Research*, *38* (2006), 6, pp. 386-404
[27] Hu, X., *et al*., On the flow around two circular cylinders in tandem arrangement at high Reynolds numbers, *Ocean Engineering*, *189* (2019), Oct., 106301
[28] Shang, J., *et al*., Numerical studies of the flow structure and aerodynamic forces on two tandem square cylinders with different chamfered-corner ratios, *Physics of Fluids*, *31* (2019), 7, 075102
[29] Tang, T., *et al*., On the transition behavior of laminar flow through and around a multi-cylinder array, *Physics of Fluids*, *32* (2020), 1, 013601
[30] Saha., Arun K., Unsteady flow past a finite square cylinder mounted on a wall at low Reynolds number, *Computers & Fluids*, *88* (2013), 15, pp. 599-615
[31] Qu, L., *et al*., Quantitative numerical analysis of flow past a circular cylinder at Reynolds number between 50 and 200, *Journal of Fluids and Structures*, *39* (2013), May, pp. 347-370

Paper submitted: July 10, 2022
Paper revised: October 1, 2022
Paper accepted: October 15, 2022